Acta Biomaterialia 108 (2020) 128–141

Contents lists available at ScienceDirect

Acta Biomaterialia

journal homepage: www.elsevier.com/locate/actbio

Full length article

Rapid fabrication of collagen bundles mimicking tumor-associated collagen architectures

Xiangyu Gong[a,c], Jonathan Kulwatno[a,b], K.L. Mills[a,c,*]

[a] Department of Mechanical, Aerospace, and Nuclear Engineering, Rensselaer Polytechnic Institute, 110 8th St, Troy, NY 12180, United States
[b] Department of Biomedical Engineering, Rensselaer Polytechnic Institute, 110 8th St, Troy, NY 12180, United States
[c] Center for Biotechnology and Interdisciplinary Studies, Rensselaer Polytechnic Institute, 110 8th St, Troy, NY 12180, United States

ARTICLE INFO

Article history:
Received 25 November 2019
Revised 10 March 2020
Accepted 12 March 2020
Available online 17 March 2020

Keywords:
Tumor microenvironment
Collagen
Hydrogels
3D culture
Microfluidics
Invasion

ABSTRACT

Stromal collagen is upregulated surrounding a solid tumor and presents as dense, thick, linearized, and aligned bundles. The collagen bundles are continually remodeled during tumor progression, and their orientation with respect to the tumor boundary has been correlated with invasive state. Currently, reconstituted-collagen gels are the standard *in vitro* tumor cell-extracellular matrix interaction model. The reticular, dense, and isotropic nanofiber (~900 nm-diameter, on average) gels do not, however, recapitulate the *in vivo* structural features of collagen bundling and alignment. Here, we present a rapid and simple method to fabricate bundles of collagen type I, whose average thickness may be varied between about 4 μm and 9 μm dependent upon diluent temperature and ionic strength. The durability and versatility of the collagen bundles was demonstrated with their incorporation into two *in vitro* models where the thickness and alignment of the collagen bundles resembled various *in vivo* arrangements. First, collagen bundles aligned by a microfluidic device elicited cancer cell contact guidance and enhanced their directional migration. Second, the presence of the collagen bundles in a bio-inert agarose hydrogel was shown to provide a route for cancer cell outgrowth. The unique structural features of the collagen bundles advance the physiological relevance of *in vitro* collagen-based tumor models for accurately capturing tumor cell-extracellular matrix interactions.

Statement of significance

Collagen in the tumor microenvironment is upregulated and remodeled into dense, thick, and aligned bundles that are associated with invasive state. Current collagen-based *in vitro* models are based on reticular, isotropic nanofiber gels that do not fully recapitulate *in vivo* tumor stromal collagen. We present a simple and robust method of rapidly fabricating cell-scale collagen bundles that better mimic the remodeled collagen surrounding a tumor. Interacting with the bundles, cancer cells exhibited drastically different phenotypic behaviors, compared to nanofiber scaffolds. This work reveals the importance of microscale architecture of *in vitro* tumor models. The collagen bundles provide physiologically relevant collagen morphologies that may be easily incorporated into existing models of tumor cell-extracellular matrix interactions.

1. Introduction

Tissue architecture, such as that provided by collagen and other fibrous proteins, profoundly influences cell behavior and functionality by providing the resident cells with structural support and mechanical cues [1,2]. Cancer cells in turn remodel collagen structures during cancer progression via contraction [3,4], crosslinking [5,6], and degradation [7]. Investigations of the tumor and tumor-stroma interface—often with second harmonic generation microscopy, but also with other methods to visualize collagen structure—have revealed upregulation of highly fibrillar collagen I. The increased density of fibrillar collagen is not restricted to a single tumor type. It has been documented for primary tumor growth

* Corresponding author at: Department of Mechanical, Aerospace, and Nuclear Engineering, Rensselaer Polytechnic Institute, 110 8th St, Troy, NY 12180, United States.
E-mail address: millsk2@rpi.edu (K.L. Mills).

https://doi.org/10.1016/j.actbio.2020.03.019
1742-7061/

in the human brain [8], prostate [9], and breast [10–12] as well as in mouse models of various different tumor types [13–18]. The upregulated collagen in the tumor environment is also remodeled into what is described as being bundles of linearized and aligned collagen fibers [12,19] with, for example, widths of bundled collagen fibers in brain tissue sections of glioblastoma multiform measuring over 2 μm [8]. In now well-known studies, Provenzano and colleagues systematically characterized the straightening and realignment of the upregulated collagen at the tumor-stroma boundary as being indicative of invasive state [13,14]. Tumor-associated collagen architecture is now being retrospectively investigated as a marker for other crucial prognostic stages, such as lymph node metastasis [20,21] and recurrence [22].

Importantly, the density, size, orientation, and organization of fibrous collagen all affect tumor cell behavior. Increased density and bundling of collagen have been correlated with increased measured stiffness of the microenvironment [10], which increases tumor cell-matrix attachment and spreading [23]. Cancer cells are observed integrated with bundles of collagen that are oriented radially to the tumor boundary, a remodeled state that is believed to favor tumor cell invasion [12,13,15]. Although collagen architecture plays an important role in cancer progression, *in vitro* models often do not recapitulate these architectural features. *In vitro* platforms that accurately capture the architecture of tumor-associated collagen are necessary to study the mechanisms of tumor cell-extracellular matrix (ECM) interactions that protect the tumor and/or aid in its progression.

Researchers often study tumor cell-ECM interactions using biological or synthetic hydrogels [24]. Given that collagen is the most abundant ECM protein [25], reconstituted type I collagen hydrogels are popular models, which are characterized by nanoscale collagen fibers physically bound to form an isotropic and porous structure [26]. Cancer cell division [27], migration [28,29], and invasive phenotypes [6,23,30] have been observed in collagen gels of varied pore size, stiffness, or crosslink density. The nanoscale, isotropic collagen fibers do not, however, recapitulate the bundling and alignment of tumor-associated collagen. The size of the fibers and pore size, until now, have only been modestly varied with collagen concentration, pH, and temperature of gelation [30–33], whereas collagen nanofibers have been aligned with an applied magnetic field [34], mechanical stretching [35], and microfluidics [36].

In order to achieve larger (microscale), aligned fibrous structures, polymeric fibers have been created by electrospinning [37,38]. When isolating the effect of fiber size on cell behavior, electrospun fibers have been shown to promote malignancy-related phenotypes from cells, for example, a mesenchymal morphology of epithelial cells [37]. Most often, electrospun fibers are created of synthetic materials that lack the ligand-binding sites of collagen for cell functions [39]. Moreover, electrospinning requires equipment that is not accessible to every lab. Alignment and feature size are also readily tunable in 2.5D micropatterned surfaces. For example, polyacrylamide gel-based microgroove topographies coated with collagen have been made to study cancer cell contact guidance and cell spreading on microscale structures [40,41]. Although the size, spacing, and alignment of the electrospun fibers or micropatterned surfaces could be systematically produced to mimic tumor-associated collagen bundle sizes and alignment, most of these models lack the 3D confinement of *in vivo* tissue.

We discovered a simple method to rapidly fabricate microscale bundles of type I collagen, with bundle sizes greater than any previously reported for *in vitro* collagen-based models. This method may be used to address the gap between current *in vitro* tumor models and *in vivo* tumor stromal architectures. We first introduce the fabrication procedure and its mechanism. The thickness of the collagen bundles was then characterized and compared to collagen fibers prepared by a traditional protocol. We further demonstrated the ability to incorporate microscale collagen bundles into two different *in vitro* systems–a 3D microfluidic device (a proposed method for aligning the bundles) and an agarose-based collagen composite gel (a proposed method for building a 3D confined model). We show these collagen bundle structures elicit cancer cell contact guidance, directional migration, and invasion differently from the traditional isotropic collagen nanofiber structures. This easy and low-cost fabrication technique of microscale collagen bundles may provide new possibilities of developing more physiologically relevant *in vitro* tumor models.

2. Materials and methods

2.1. Collagen matrix preparations

Eight parts of type I bovine collagen monomer solution (3.0 mg/mL, pH 2, PureCol, Advanced BioMatrix, USA) were mixed with one part of 10 × phosphate-buffered saline (PBS). The solution was then neutralized to a pH of ~7.4 with about one part of 0.1 M sodium hydroxide (NaOH) solution. Neutralization was conducted on ice. The collagen concentration of the neutralized solution was 2.4 mg/mL. In this study, we prepared all the samples with different collagen structures by mixing the same quantity of water or PBS, to produce a final collagen concentration of 1.2 mg/mL.

For the ease of description, here we term the commonly used, traditional collagen gelling protocol (based on the manufacturer's manual) as "Fiber method" and our novel collagen bundle fabricating protocol as "Bundle method" (Fig. 1). For the fiber method, we thoroughly mixed a 2.4 mg/mL neutralized ice-cold collagen solution with the same amount of cold ultrapure water with a vortex mixer for ~ 30 s. This diluted 1.2 mg/mL collagen precursor was then allowed to polymerize into an isotropic collagen nanofiber gel in a 37 °C, humidified incubator. For the bundle method, instead of cold water, we vortex-mixed a neutralized collagen solution with the same volume of pre-warmed ultrapure water for 30 s. Visible collagen bundles appeared instantly after the mixing procedure. More details on our collagen bundle fabrication method are presented in the Results section. For the cell migration study, we coated a glass bottom dish with a PBS-diluted PureCol solution (dilution ratio: 1:30) at 37 °C for 3 h. We also produced aligned collagen nanofibers (1.2 mg/mL) following the method developed by Kim and colleagues [42] (Fig. S3).

2.2. Rat tail collagen extraction

Rat tail collagen was also used to demonstrate the collagen bundle fabricating technique. Sprague Dawley adult female rat tails were generously provided by Dr. Ryan Gilbert's lab at RPI. Tails were initially frozen at −80 °C until processed. Tails were thawed at 4 °C overnight the day before extraction. For extraction, protocols similar to Ritte and Rajan *et al.* were used [43,44]. Pliers were used to isolate the tail tendons, which were then submerged into a beaker of 1 × PBS on ice. When all tails were processed, the tail tendons were rinsed three times with cold deionized water. Then, tail tendons were transferred to a new beaker containing 20 mM acetic acid, at a volume of 200 mL per tail. This beaker was placed on a magnetic stir plate with a stir bar at 4 °C and allowed to stir for 3 days. After, the solution was poured into 250 mL centrifuge bottles and centrifuged for 45 min at 10,000 × *g* at 4 °C. The supernatant was collected into 50 mL centrifuge tubes and frozen at −80 °C overnight. The collagen solution was then lyophilized using a CentriVap (Labconco) and vacuum (Fisher) for 5 days. The resulting collagen mesh was collected, weighed, and resuspended at the concentration of 15 mg/mL in fresh 20 mM acetic acid in a glass

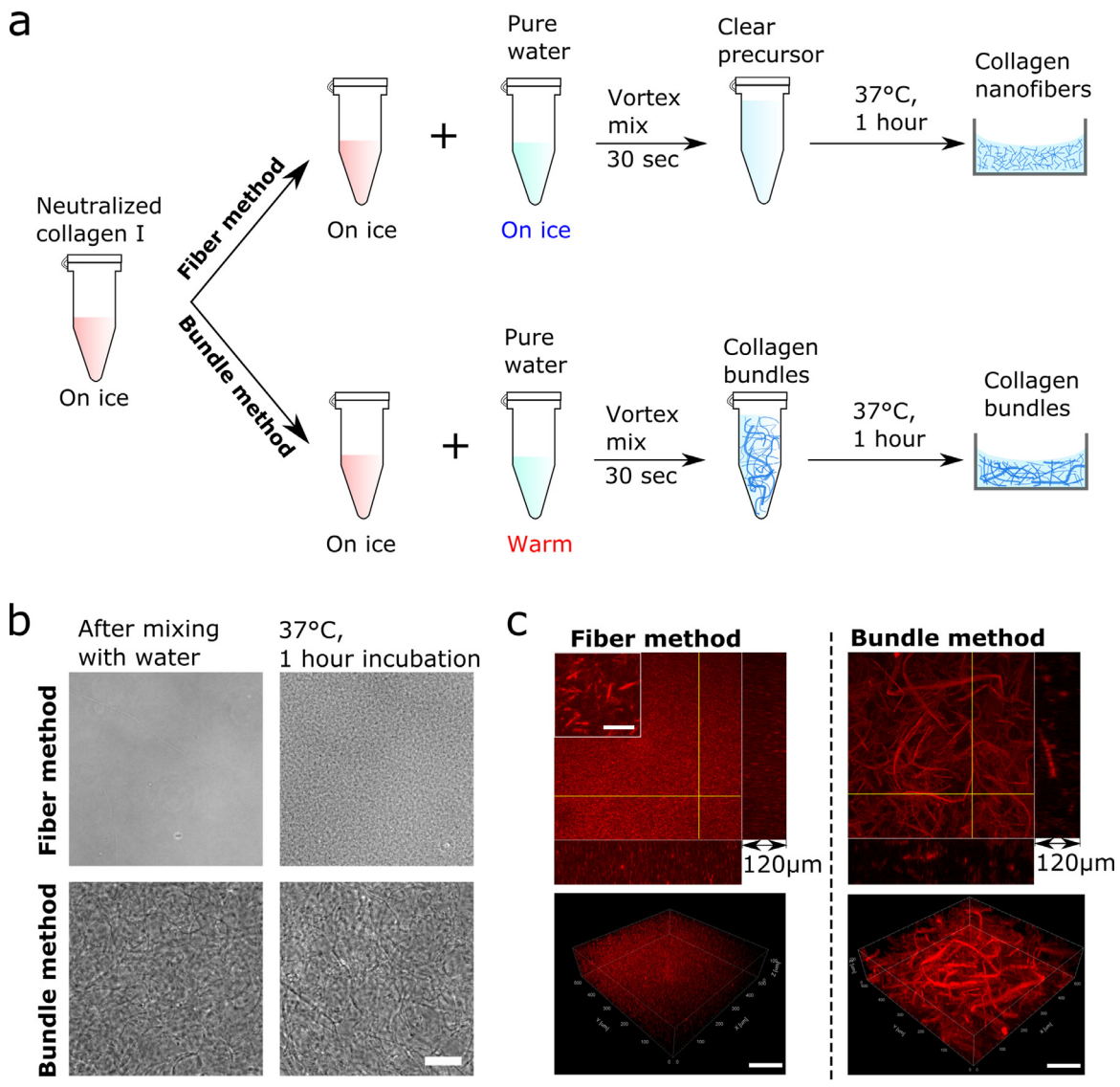

Fig. 1. Rapid fabrication of collagen bundles compared with collagen fiber gels. (a) The common procedure to prepare a collagen fiber gel (fiber method) *versus* the rapid fabrication of collagen bundles (bundle method). (b) Brightfield images comparing the appearance of the collagen-water solutions mixed using the fiber and bundle methods before and after incubation for an hour at 37 °C. Scale bar: 100 μm. Using the fiber method, a clear solution of collagen and cold water polymerized into a collagen gel with dense fibrous structures after incubation. In the bundle method, visible bundles instantly formed after mixing with warm water (40 °C) and remained after the one-hour incubation. (c) Confocal reflectance images of collagen fibers (scale bar in inset: 10 μm) and collagen bundles made by the respective methods. Scale bars in 3D reconstructions: 100 μm.

vial and kept at 4 °C. To sterilize, chloroform was added at 10% of the volume and allowed to incubate overnight at 4 °C, where after the collagen solution was aseptically transferred into a sterile centrifuge tube. Purity of the collagen was verified via SDS-PAGE and mass spectroscopy by comparison of a commercially available rat tail collagen solution (Invitrogen).

2.3. Design and fabrication of the microfluidic chamber

We designed micro-post array patterns using the computer aided design (CAD) software SolidWorks (Dassault Systèmes), and the patterns were printed on a chrome mask by a high-resolution printing service (Front Range Photo Mask, CO, USA). A rectangular feature (thickness: 70-μm) with micro-wells in it was fabricated on a silicon wafer using a negative photoresist (SU-8 3050, MicroChem, MA, USA), through the techniques of photolithography. The standard fabricating guideline is provided by the SU-8 manufacturer. After the fabrication, we inspected the depth of the microwells by a stylus profilometer (Veeco, DekTak 8). We then molded the micro-post-containing rectangular chamber on the silicon master with polydimethylsiloxane (PDMS, Sylgard 184, Dow Corning) following standard soft lithography techniquess[45]. After the PDMS was fully cured, we peeled it off and trimmed it to fit in a glass-bottomed cell culture dish. Before attaching the PDMS chamber onto the glass bottom, we treated the chamber in a plasma cleaner (Harrick Plasma) to make the PDMS surface hydrophilic. All the PDMS components were sterilized with 70% ethanol and then under UV light for at least 30 min.

2.4. Cell culture

In this study, we used an invasive breast cancer cell line MDA-MB-231, a human colon cancer cell line HCT-116, and a green fluorescent protein (GFP)-labeled MDA-MB-231 (a kind gift from Dr. Mihaela Skobe at Icahn School of Medicine at Mount Sinai). MDA-MB-231 and GFP-MDA-MB-231 cells were cultured in RPMI 1640 medium supplemented with 2 mM L-glutamine (Gibco), 10% FBS (Gibco), and 1% penicillin/streptomycin (Gibco). HCT-116

cells were cultured in McCoy's 5A medium with 10% FBS and 1% penicillin/streptomycin. All cells were incubated in humid air maintained at 37 °C and 5% CO_2. The cell culture medium was changed every 2–3 days and the cells were passaged when they reached 90% confluency. For the 10-day cell culture in agarose-collagen co-gels, the cell culture medium was changed every three days.

2.5. Preparation of agarose and agarose-collagen co-gels

Low gelling temperature agarose powder (Sigma) was dissolved in ultrapure water or 1 × PBS in a 95 °C water bath for 15 minutes. When fully dissolved, the water-based or PBS-based agarose solutions were kept in a 40 °C water bath. The initial concentrations (wt/vol%) of the agarose solutions were 0.6% and 1.2%. In this study, we prepared three types of hydrogels at two final agarose concentrations: 0.3% and 0.6% pure agarose gels, 0.3% and 0.6% agarose-collagen fiber co-gels, and 0.3% and 0.6% agarose-collagen bundle co-gels. To make pure agarose, we diluted water-based 0.6% or 1.2% agarose solution with the same amount of 40 °C PBS (1 ×). To prepare agarose-collagen fiber co-gels, the collagen solution was first neutralized on ice (2.4 mg/mL) as described above. To minimize local gelation of agarose when it contacts the ice-cold neutralized collagen, the collagen solution was pre-warmed to 37 °C for 5 min—during which no perceptible collagen polymerization occurred (Fig. S7). We then thoroughly mixed the pre-warmed collagen solution with the same volume of PBS-based 0.6% or 1.2% agarose solution to produce agarose concentrations of 0.3% or 0.6%, respectively. For agarose-collagen bundle co-gels, we mixed the pre-warmed neutralized collagen solution with the same amount of water-based 0.6% or 1.2% agarose solution. Collagen bundles instantly appeared in pure water-based agarose precursor. In the described co-gel protocols, the final collagen content of both co-gels was 1.2 mg/mL. To grow cells in these gels, we quickly mixed a negligible volume of cell suspension at a cell density of 70,000 cells/mL in the gel precursors before they gelled.

2.6. Mechanical characterization of agarose and agarose-collagen co-gels

The mechanical characterization of the three gel types (pure agarose gels, agarose-collagen fiber co-gels, and agarose-collagen bundle co-gels) was performed on a high-precision piezo-electric actuator-controlled indentation system (CellScale, Canada). A small glass bead (radius $R = 1.5$ mm) attached on the end of a tungsten cantilever was used to indent the hydrogel samples. The indentation depth, d, was recorded by a camera and the indentation force, F, was computed based on the measured deflection and known bending rigidity of the cantilever. Using a MATLAB code, the experimental indentation force-depth curves were then fit with the Hertz contact model (Eq. (1)) for a rigid spherical indenter contacting a flat surface. The elastic modulus, E, of the hydrogel was calculated from this fit. The Poisson's ratio, , was taken to be 0.49.

$$F = \frac{4}{3}\frac{E \cdot R^{1/2}}{(1-\nu)^2} \cdot d^{3/2} \quad (1)$$

2.7. Immunofluorescence staining

The cell-laden hydrogel samples were washed in PBS, fixed with 4% paraformaldehyde at 37 °C for 40 min, and permeabilized with 0.5% Triton X-100 at 37 °C for 40 min. After washing with PBS three times for 30 min, the samples were blocked overnight in 5% BSA in PBS at room temperature. The samples were then incubated with rhodamine phalloidin (1:50, R415, Thermo Fisher) and Hoechst (0.5 μg/mL, Hoechst 33342, Thermo Fisher) protected from light and maintained at 4 °C overnight.

2.8. Western blotting

To assess the expression of proteins associated with epithelial and mesenchymal phenotypes, western blotting was performed. HCT116 and MDA-MB-231 whole cell lysates were isolated from flasks using mammalian protein extraction reagent (M-PER; ThermoFisher) following manufacturer protocols. Samples were treated with NuPAGE LDS Buffer (ThermoFisher) and NuPAGE reducing agent (ThermoFisher), and were heated to 70 °C for 10 min. Protein separation was done through electrophoresis using a NuPAGE 3–8% tris-acetate gel (ThermoFisher) with wells loaded with 10 µg of protein. Subsequently, proteins were transferred onto a nitrocellulose membrane and then blocked overnight while shaken at 4 °C in TBST-5% BSA – a TBS Tween-20 (TBST; ThermoFisher) solution containing 5% bovine serum albumin (BSA; Sigma).

Primary antibodies for vimentin (1:5000; Santa Cruz Biotechnology), E-cadherin (1:2000; Cell Signaling Technology), and GAPDH (1:15,000; Cell Signaling Technology) were diluted in TBST-5% BSA. The diluted primary antibodies were applied to appropriate sections of the membrane overnight while shaken at 4 °C. Membrane sections were washed overnight while shaken at 4 °C in TBST. Horseradish peroxidase-conjugated secondary antibodies (Cell Signaling Technology) diluted in TBST-5% BSA were then applied for 1 h. Secondary antibody dilutions were 1:10,000 for vimentin, 1:2000 for E-cadherin, and 1:15,000 for GAPDH. Bound antibodies were detected using SuperSignal West Pico PLUS Chemiluminescent Substrate (ThermoFisher). Imaging was performed using a Chemidoc XRS+ system (BioRad). Quantification of band parameters were performed using the associated Image Lab software (BioRad).

2.9. Image acquisition

All bright field images of collagen fibers and bundles were obtained with an inverted microscope (Zeiss, Axio Vert.A1). Fluorescence images of cancer cells/tumor spheroids and reflectance images of collagen microstructures were acquired with laser scanning confocal microscopes (Leica SP8 or Zeiss LSM 510 META). Live confocal imaging of MDA-MB-231 seeded on 2D glass or embedded in collagen bundles or in collagen fibrous gels was conducted in an environmental chamber (Okolab) using a Leica SP8 for 5 h with image volumes captured at 15 min intervals.

2.10. Scanning electron microscopy

Scanning electron microscopy (SEM) was used to characterize the microscopic structural differences between collagen fibers and bundles. The collagen fibrous gel prepared by the fiber method and the collagen bundles prepared by the bundle method were first fixed in glutaraldehyde at 4 °C overnight. The samples were then dehydrated using a chemical drying method [46]. In brief, after carefully rinsing the fixed samples with ultrapure water, we dehydrated the samples with a series of aqueous ethanol solutions: 50%, 75%, 80%, 90%, and 100%. The samples were allowed to stay in each ethanol concentration for 5 min and each ethanol concentration was applied twice. After the water in the samples was completely replaced by 100% ethanol, the samples were then plunged into hexamethyldisilazane (HMDS) for 40 min. Lastly, the HMDS was removed and the samples were air-dried. The dehydrated collagen fibers and bundles were sputter coated with platinum using a Denton Desk IV sputter coating system and imaged with a Zeiss SUPRA 55 FESEM in the Microscale and Nanoscale Cleanroom (MNCR) at Rensselaer Polytechnic institute.

2.11. Image analysis and statistical analysis

Length measurements from any brightfield or confocal image were performed using ImageJ (NIH) [47]. Thicknesses of collagen fibers and bundles in confocal images were measured with the ImageJ plugin "Ridge Detection" [48]. Orientation of the microfluidics-aligned collagen bundles was characterized using the ImageJ plugin "OrientationJ" [49]. The visualization and surface analysis software Imaris 9 (Oxford Instruments) was used to reconstruct confocal image stacks from which cell migration in 3D was automatically tracked and tumor volume was automatically computed. Data was presented as bar plots showing mean ± standard deviation (s.d), or as box plots, where boxes represent the 25th to 75th percentile with a median line, and whiskers represent the 1.5 interquartile range (IQR). Statistical difference between multiple experimental conditions was determined by one-way or two-way ANOVA tests with Tukey post hoc testing. Differences were considered significant at $p < 0.05$.

3. Results

3.1. Rapid fabrication of microscale collagen bundles

Toward the need for physiologically relevant *in vitro* ECM models, we present a procedure to rapidly fabricate microscale collagen bundles. The common method (termed "fiber method", Fig. 1(a)) of preparing collagen hydrogels includes three steps: (i) neutralization of the collagen monomeric stock solution (pH = ~7.4, on ice, see detwails in Materials and Methods), (ii) adjustment of the collagen concentration by addition of ice-cold water, and (iii) gelation at 37 °C for at least an hour. With this method, a thoroughly mixed, clear collagen precursor gradually polymerizes into a gel consisting of dense reticular collagen fibers that are on the order of hundreds of nanometers in thickness. In contrast, using the "bundle method" (Fig. 1(a)), we found that replacing the ice-cold water in step (ii)—adjustment of collagen concentration—with warm water (tested temperature range: 25–60 °C) resulted in visibly thick collagen bundles appearing instantly after mixing. The bundled collagen remained after an extended incubation at 37 °C. Phase contrast microscope images (Fig. 1(b)) show the appearance of collagen solutions at the different steps of the fiber and bundle methods, corresponding to Fig. 1(a). The bundle method in Fig. 1(b) was carried out with warm water at 40 °C. The drastic structural differences were further visualized in confocal reflectance images (Fig. 1(c)).

3.2. Investigating the mechanism of collagen bundle formation

Comparing the fiber and bundle methods, it is clear that introduction of *warm* water to the ice-cold neutralized collagen solution played a key role in the collagen bundle formation. To investigate the role of temperature in collagen bundle formation, we mixed ice-cold neutralized collagen solution with the same amount of pure water at incremental temperatures: 25 °C (room temperature), 40 °C, and 60 °C. We also briefly pre-warmed the neutralized collagen to 37 °C and mixed it with 40 °C water. These varied conditions yielded different morphologies of collagen bundles which are similar to collagen bundles observed *in vivo* (Fig. 2(a)). Thickness characterization of the collagen bundles revealed a positive correlation between pure water temperature and bundle thickness (Fig. 2(b)).

To further investigate the bundling mechanism, we replaced the warm water with warm (40 °C) PBS at concentrations of 1 × and 0.25 ×, which introduced a higher ionic strength due to the dissolved salts (morphologies shown in Fig. S1). Interestingly, mixing neutralized collagen with pre-warmed 1 × PBS did not produce any instant collagen bundles. After a 1-h incubation, the precursor turned into a gel with dense, reticular collagen fibers with thicknesses statistically similar to those produced by the fiber method (Fig. 2(b)). However, mixing neutralized collagen with 0.25 × warm PBS resulted in a precursor with a "transitioning state" – a small amount of short bundles floating in a clear solution (Fig. S1(b)) and yielded slightly thicker collagen fibers in the gel after the incubation (Fig. 2(b)). Therefore, for collagen bundle formation, both increased temperature and low ionic strength of the diluent are necessary.

To better understand the microscopic structure of the collagen bundles we produced, the samples were imaged with a scanning electron microscope (SEM, Fig. 2(c)) – the much thicker collagen bundles were found to be composed of multiple long collagen fibers that coiled together, similar to *in vivo* observations [13,40]. In addition, we demonstrated that the bundle method is not restricted to the bovine collagen utilized here, but functions the same using type I collagen isolated from other species (*e.g.*, rat tail, Fig. S2).

3.3. Microfluidics-driven patterning and alignment of collagen bundles

After fabrication, the collagen bundles were randomly and loosely packed in a much lower concentration of collagen solution that did not form a hydrogel like the fiber method. Since they were not bound in a hydrogel, these micro-scale collagen bundles could be used to form large-scale, complex patterns with controllable curvature and local alignment. We aligned the bundles post-production into different micro-scale curvatures using a microfluidics method (Fig. 3). A PDMS microfluidic chamber (width: 15 mm, height: 70 μm) with arrays of cylindrical (diameter: 70 μm) and triangular (equilateral, side length: 830 μm) micro-posts was made. The chamber had an open end where the collagen bundles were introduced, and tubing was sealed to a port on the opposite end so that a vacuum could be applied across the chamber (Fig. 3(a)). A syringe was attached to the free end of the tubing and used to apply a gentle vacuum to pull a solution containing the collagen bundles through the chamber. The long collagen bundles were captured by the micro-posts and the flow facilitated the alignment of the free ends of these bundles (Fig. 3(b)). The combination of the micro-posts' geometric features and the direction of the flow arranged the collagen bundles into unique patterns (Fig. 3(c)). When observing the collagen bundles around a micro-post, we found that the bundles were locally aligned, and the orientation of their local alignment was determined by the cross-sectional geometry of the micro-post (Fig. 3(d)).

3.4. Collagen bundle arrangement facilitates cell contact guidance

The patterned microscale collagen bundles resembled the alignment of thick collagen bundles observed from *in vivo* studies [15,40], specifically tumor-encircling alignment in regions where the bundles wrap the microposts and radial alignment where the collagen bundles were aligned only by flow (Fig. 4(b)). To investigate the interactions between cancer cells and the patterned collagen bundles, we flowed metastatic breast cancer cells MDA-MB-231 (GFP-labeled) with the collagen bundles through the microfluidic chamber. After patterning the flow was halted, and the cells were cultured *in situ* for one week. Not only did the cancer cells elongate along the aligned collagen bundles adopting the bundle curvature (Fig. 4(a)), but upon closer inspection it can be seen that the cancer cells inserted themselves in between the collagen bundles (Fig. 4(b) and (c)). When caught by the micro-posts from the flow, the bundles distributed themselves over the entire height of the micro-posts creating arrangements of bundles multiple layers

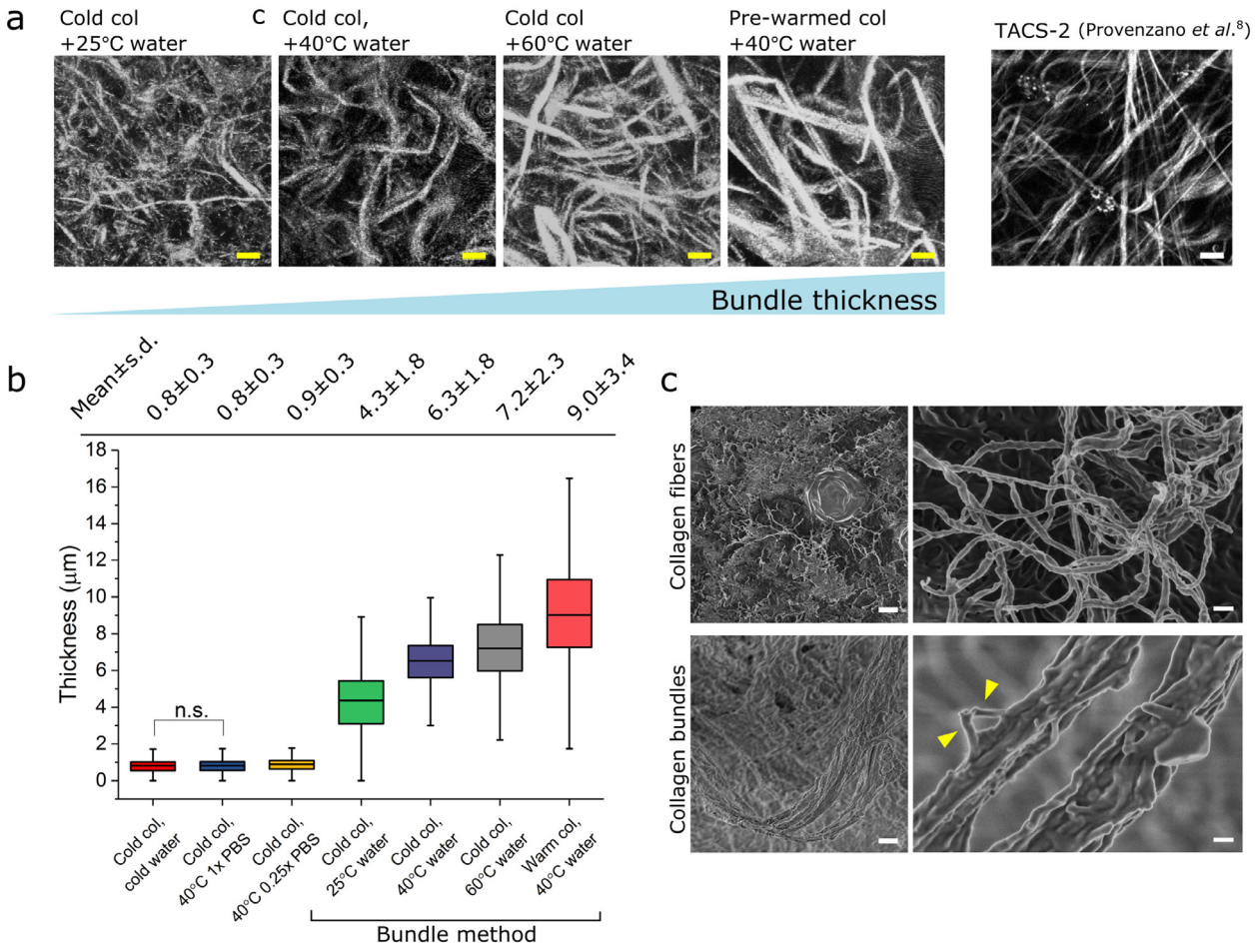

Fig. 2. Morphological characterizations of collagen bundles compared to collagen fibers. (a) Confocal reflectance imaging of collagen bundles prepared at different temperatures, in comparison with an *in vivo* tumor-associated collagen signature example (TACS-2) from Provenzano et al. [13] (multiphoton excitation/second harmonic generation image, reproduced from Provenzano et al. [13]), scale bars: 25 μm. (b) Characterizing the thickness of collagen fibers and bundles prepared by different protocols. Mean thickness and the standard deviation (s.d.) are listed above the corresponding condition. One-way ANOVA with Tukey post hoc testing was performed. Significant difference ($p < 0.005$) was detected between any two of the conditions, except the two groups marker with "n.s.". ($n \geq 1731$ measurements, three samples each condition). Boxes represent 25th to 75th percentile and whiskers represent 1.5 IQR. (c) SEM images of microscopic structures of single collagen fibers (top row) and collagen bundles that consist of multiple bundled collagen fibers (bottom row). Scale bars: 2 μm (left column); 200 nm (right column). Arrowheads indicate free ends of collagen fibers in a collagen bundle.

in height as well as thickness (radially from the center of the post). The cancer cells were able to migrate between the collagen bundles (Fig. 4(d)) because the spacing between the aligned collagen bundles was on the order of a few tens of micrometers, which is approximately the size of a single cell (Fig. 4(e)). With this assay we showed that the 3D aligned collagen bundles enabled cancer cell contact guidance.

3.5. Aligned collagen bundles enhance cell motility and directional migration

After establishing cancer cell contact guidance in the 3D aligned collagen bundles, we characterized the migration of the cancer cells in the 3D aligned collagen bundles compared to three other common experimental models: 2D collagen-coated glass, 3D dense isotropic collagen fibers (1.2 mg/mL), and 3D strain-induced aligned collagen fibers (method to alter alignment of isotropic fibers adopted from Kim *et al.* [42], details in Fig. S3). After 24-h of culture, we imaged GFP-labeled MDA-MB-231 cells in these four conditions (Fig. 5(a)) every 15 min for five hours using confocal 3D live imaging (Fig. 5(b), Movie S1). Both persistence and migration speed of the cells in the four conditions were characterized.

To compare the persistence of cells migrating under these collagen conditions, we used the cell directedness, defined as the ratio of cell displacement to the trajectory length [50] (also see Figs. S4 and 5(d)). The cell directedness measurement is lowest for the cells embedded in the isotropic collagen fibers, which indicates they were least persistent. In comparison, the directedness values of the cells in both aligned collagen bundles and aligned collagen fibers were significantly enhanced, which corresponds to more cells that were guided to migrate along the alignment. To compare migration speeds, we calculated the average frame-to-frame cell speed (the displacement of a cell between two frames divided by the time interval, 15 min) under each condition (Fig. 5(d), Movie S2). Expectedly, without constraint in the third dimension the cells on the collagen-coated glass surface were most mobile; they moved fastest at a mean speed of 0.63 μm/min. The cells in all three 3D collagen conditions were significantly slower than those on the 2D glass. The mean speed of the cells in aligned collagen bundles (0.22 μm/min) was the second fastest, significantly faster than the cells in aligned dense collagen fibers (0.19 μm/min) but comparable with the mean speed of cells embedded in dense isotropic collagen fibers (0.2 μm/min). The measurements on directedness and speed are consistent with the observations (Supplementary movies) that (1) cells in 3D collagen were slower than on the 2D

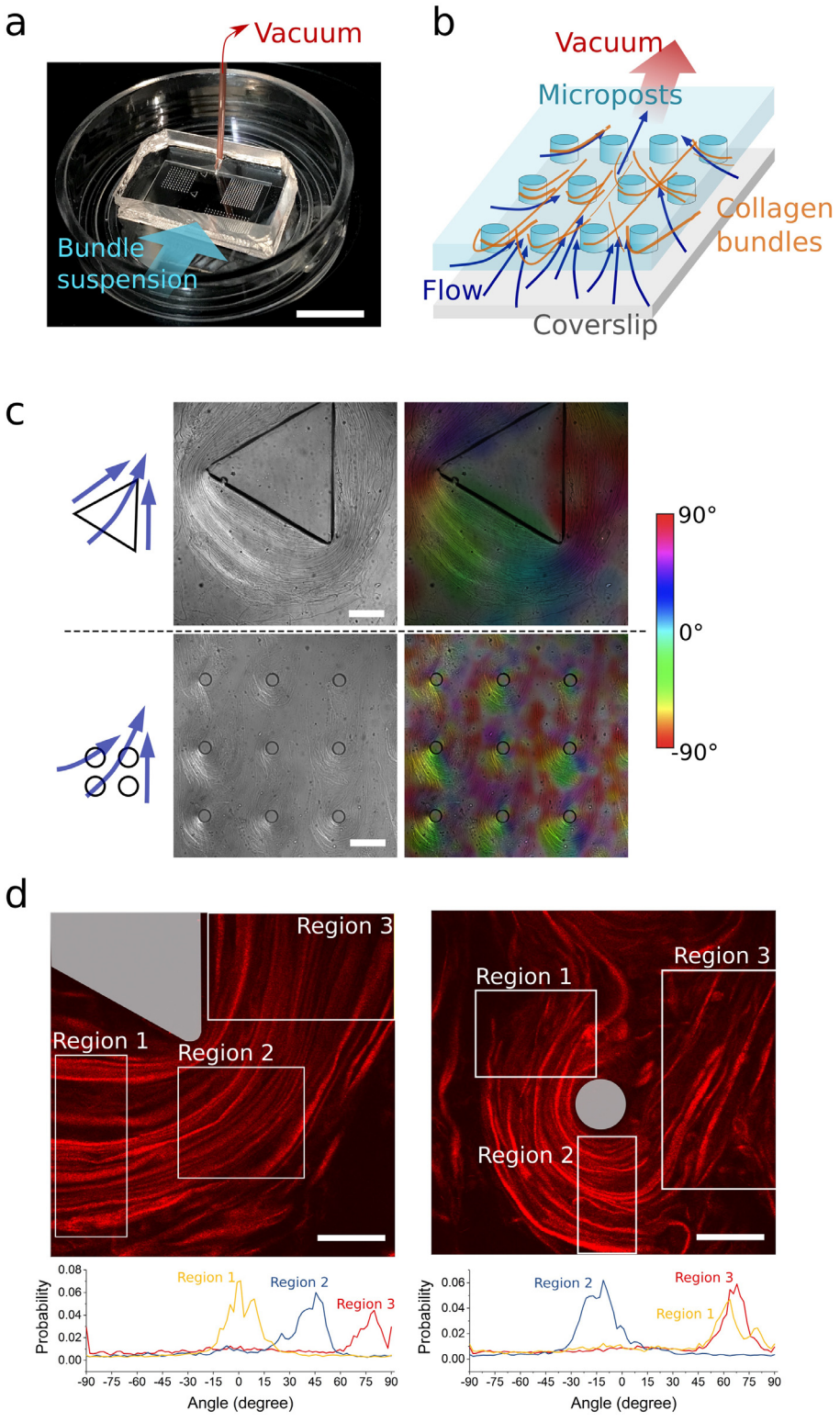

Fig. 3. Microfluidics-driven patterning and alignment of collagen bundles. (a) Microfluidic chamber containing micro-post arrays. A suspension of collagen bundles was introduced at the open end and a vacuum was applied through the tubing sealed to the opposite end. The vacuum pulled the suspension through the microfluidic chamber. Scale bar: 10 mm. (b) Schematic showing the design of the microfluidic chamber and direction of microfluidic flow carrying collagen bundles that get captured by and align around an array of micro-posts. (c) Large-scale differential interference contrast (DIC) images of collagen bundles near micro-posts of varying shapes (left) and their respective colormaps that denote bundle orientation (right). Blue arrows indicate the flow direction corresponding to the DIC images. Scale bars: 200 μm. (d) Confocal images of collagen bundles around micro-posts of different shapes. Cross-sections of the micro-posts are highlighted in gray. Below the confocal images we show the orientation characterizations of the bundles in multiple regions in each image. Scale bars: 100 μm.

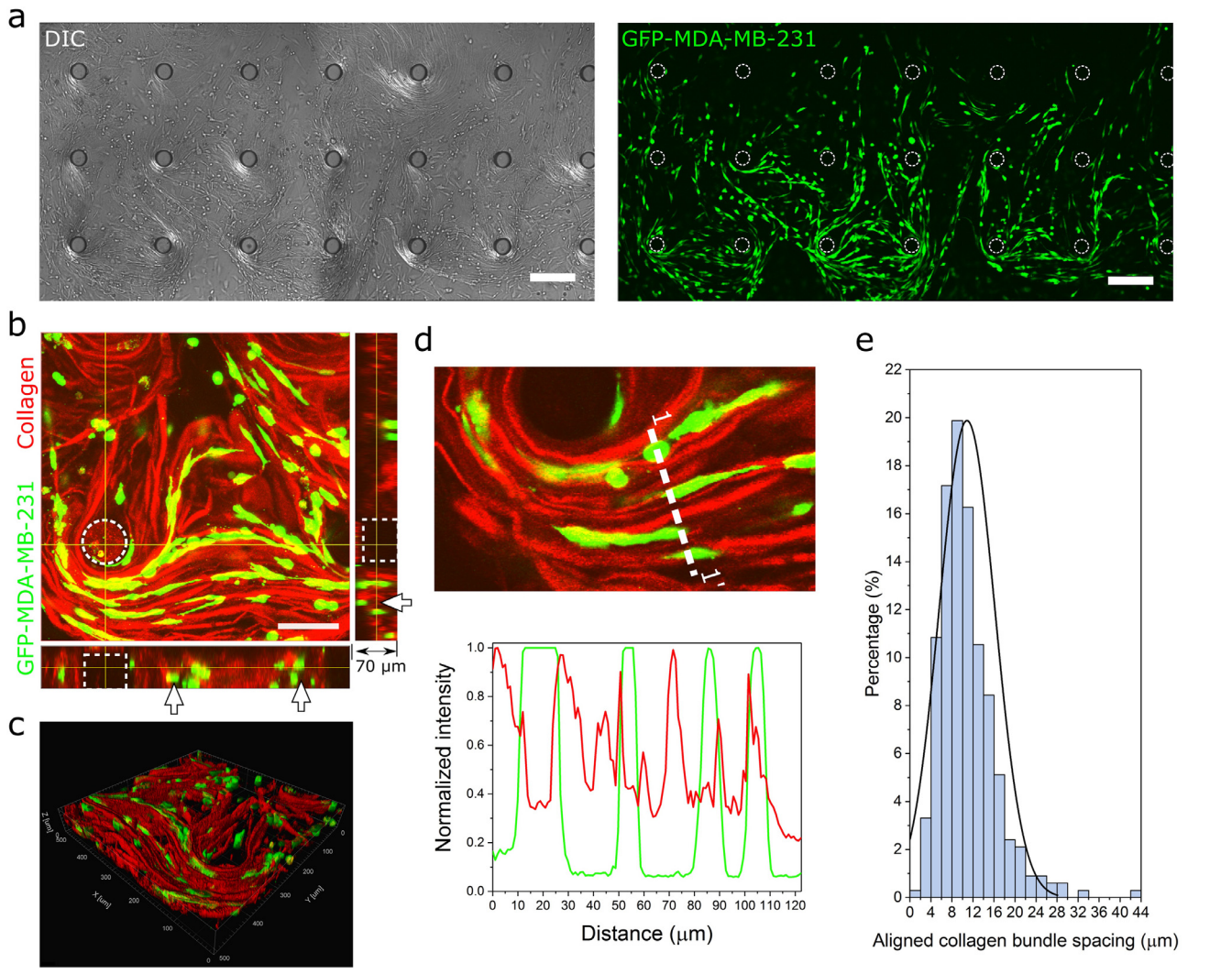

Fig. 4. Complex collagen bundle topography facilitates cell contact guidance. (a) DIC images (left) and confocal images (right) showing large scale collagen bundle topographic landscape guiding directional elongation of GFP-labeled MDA-MB-231 cells. Scale bars: 200 μm. (b) Confocal image volume showing cells reoriented to the local collagen bundle structures. Arrows indicate the cells and collagen bundles were distributed through the height of the microfluidic chamber. (c) 3D reconstruction of cell contact guidance in collagen bundle topography. (d) Spatial characterization showing that cancer cells insert themselves in between the collagen bundles, mimicking *in vivo* observations. (e) Spacings between collagen bundles measured from confocal reflectance images (n = 332 measurements, mean ± standard deviation: 10.9 ± 5.3 μm).

collagen-coated glass; (2) most cells in the isotropic collagen fibers did not migrate away but oscillated near their original positions at a significant speed; (3) aligned collagen bundles and the alignment of collagen fibers guided more cells to migrate persistently, but the cells migrated faster along the bundles than the aligned dense fibers.

Cell speed and persistence can be also corroborated by visualizations of *in situ* cell trajectories (Fig. 5(b)) and three-dimensional wind rose plots (Fig. 5(c)). Five-hour long trajectories are superimposed onto the respective collagen structures in Fig. 5(b). The cells on 2D collagen-coated glass migrated the furthest and their trajectories were random, while the trajectories of most cells in the collagen bundles and aligned dense fibers matched the local aligned topography. In comparison, the cells embedded in isotropic collagen fibers were less migratory and their trajectories extended least into the collagen matrix. Visualizing more trajectories ($n \geq 81$) as 3D wind rose plots confirms the relatively long but tortuous migration paths of the cells on 2D glass and the more directed motion of the cells migrating in the bundles or in the aligned fibers compared to the constrained cell movement in isotropic collagen fiber gel (Fig. 5(c)). These results indicate that aligned collagen bundles enhance the speed and the translocating capability of the cells in 3D over the nanofiber-based collagen gels.

3.6. *Agarose-collagen bundle co-gels as a platform for recapitulating carcinoma cell* in vivo *phenotypes*

Having shown that collagen structure and dimensionality influenced cancer cell motility, we then investigated whether collagen structure plays a role in model tumor growth. We chose to grow the model tumors in collagen-agarose co-gels since the mechanical stiffness is weakly dependent upon the collagen fraction [51,52] and the interaction with collagen is confined within a 3D gel matrix. Specifically, three types of hydrogels/co-gels were prepared: (i) pure agarose, (ii) agarose-collagen dense fiber co-gel, and (iii) agarose-collagen bundle co-gel (Fig. 6(a)). We used two agarose concentrations—0.3% and 0.6% (wt/vol)—to recapitulate the stiffness of normal tissue and cancerous tissue, respectively. Collagen content was kept constant in all co-gels, at 1.2 mg/mL, to, as closely as possible, only vary the collagen structure. In Fig. 6(a) visual comparisons of the gel structures may be seen at different length scales.

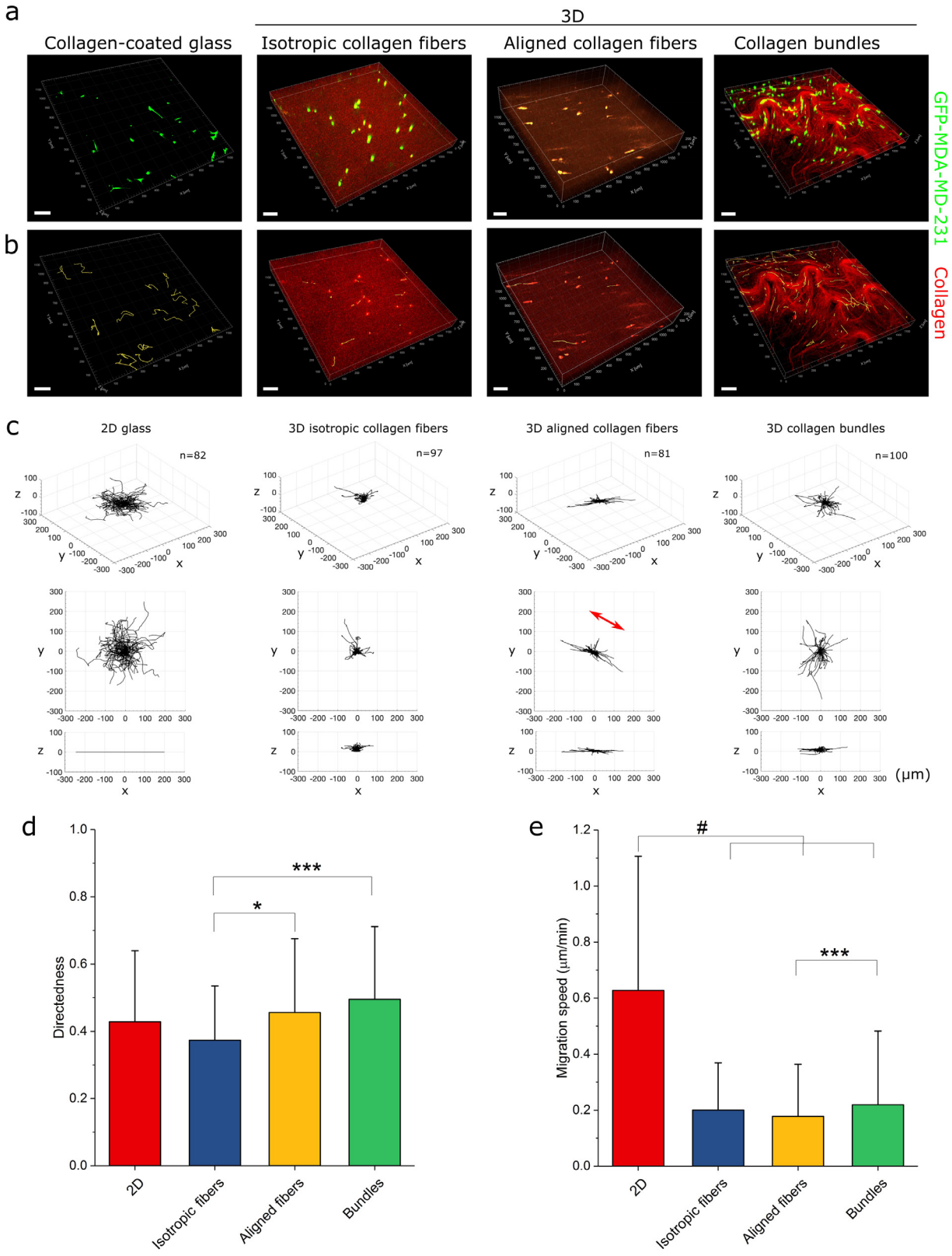

Fig. 5. Cancer cell migration characterization under varied collagen structural conditions. (a) Confocal images of GFP-labeled MDA-MB-231 cells seeded on collagen-coated glass, in dense isotropic collagen nanofibers, in dense aligned collagen nanofibers, and aligned collagen bundles. (b) *In situ* migration tracks of GFP-labeled MDA-MB-231 cells under the four culture conditions over five hours. Yellow lines denote the cell migration trajectories. Scale bars: 100 μm. (c) Three-dimensional cell trajectory plots comparing cell migration patterns under the four conditions. Red arrow indicates the orientation of the aligned collagen fibers. (e) Directedness of the cells over a five-hour period ($n \geq 81$ tracks). (d) Frame-to-frame cell migration speeds between 15-minute time interval ($n \geq 1696$ measurements of at least 81 cells). One-way ANOVA with Tukey post hoc testing was performed. * $p < 0.05$, $^{***}p < 0.0005$, # $p < 0.0001$.

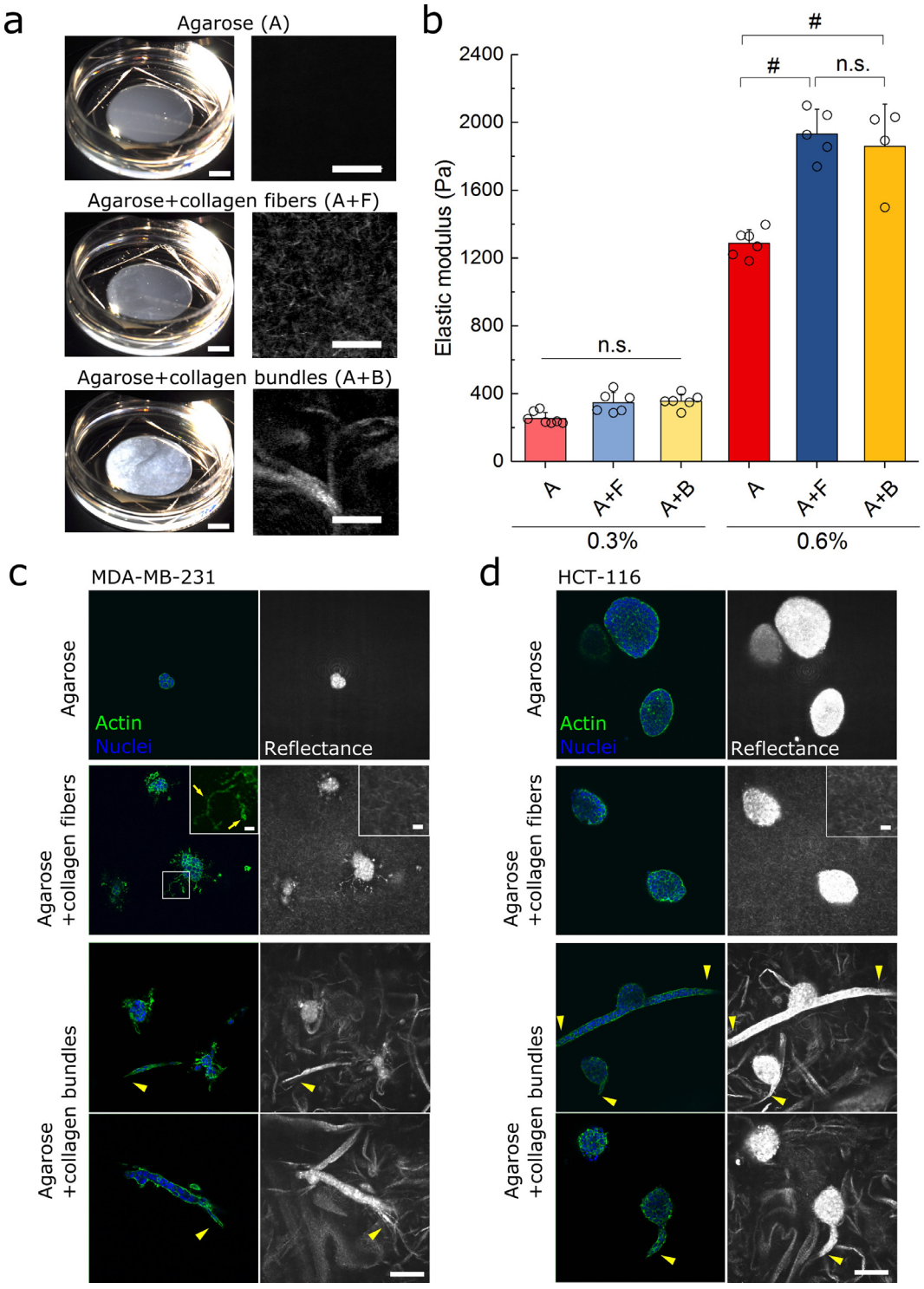

Fig. 6. Agarose-collagen based 3D composite hydrogels as *in vitro* tumor models with tunable collagen structures. (a) Macrographs (left column, scale bars: 5 mm) and confocal images (right column, scale bars: 50 μm) of three types of gels: 0.3% (w/v) agarose (A), 0.3% agarose +1.2 mg/mL collagen fiber co-gel (A + F), 0.3% agarose +1.2 mg/mL collagen bundle co-gel (A + B). (b) Elastic modulus characterizations of the three gel types with two different agarose concentrations. No significant difference was detected in the elastic moduli of the gels at the lower (0.3%) agarose concentrations. At 0.6% agarose concentration, pure agarose was significantly softer than its corresponding agarose-collagen co-gels. (Two-way ANOVA with Tukey post hoc testing, $n \geq 4$ for each gel type, # $p < 0.0001$, n.s.: no significance). (c) MDA-MB-231 tumor growth (Day 10) in the three gel types at 0.3% agarose concentration. Scale bar: 100 μm. Insets show the filopodia (yellow arrows) extending into the surrounding agarose-collagen fiber matrix. Scale bars in insets are 10 μm. (d) HCT-116 tumor growth (Day 10) in the three gel types at 0.3% agarose concentration. Scale bar: 100 μm. All the arrowheads indicate the multicellular invasive growth along collagen bundles.

We first measured the elastic moduli of the hydrogels (Fig. 6(b)) by milli-indentation. The three gels containing 0.3% agarose had no significant difference in mean elastic moduli values, which were between 254 Pa and 356 Pa (Fig. 6(b)). This range is similar to that reported for healthy mammary tissue [53]. The three gels containing 0.6% agarose were about five times stiffer than the 0.3% gels (1288–1932 Pa), which is on the order of breast tumor tissue [53]. Interestingly, incorporating collagen, either as fibers or bundles, into the 0.6% agarose gels significantly, although modestly, increased the macroscopically measured elastic moduli of both co-gels (Fig. 6(b)). This was likely due to the increased density and smaller pore size preventing the sliding of collagen fibers through the agarose mesh [51]. Here we focus on analyzing the growth in the softer, 0.3% agarose and its co-gels. The cancer cells proliferated more in the softer gels (as previously observed [54]) and the increased growth made the trends, which were common to both the 0.3% and 0.6% sets of gels, more prominent. Growth in the 0.6% agarose and its co-gels is shown in Fig. S5.

Breast cancer cells (MDA-MB-231) and colon cancer cells (HCT-116) were randomly embedded as single cells and cultured in the three gel conditions. As shown in literature [55,56], these two cell lines of epithelial origin have different metastatic potentials: the MDA-MB-231 cell line is known to have a higher metastatic potential, whereas the HCT-116 cell line retains more epithelial characteristics (also see expression of epithelial-mesenchymal transition markers in Fig. S6) . After the cells were encapsulated in these gels, they appeared morphologically identical in all gel conditions and we did not observe any interaction between the embedded cells and the neighboring collagen bundles (Fig. S7). After 10 days of growth in the matrices the cells were fixed, and their F-actin and nuclei were stained so that their interactions with the matrices could be visualized (Figs. 6(c), (d) and 7).

The growth behavior and morphologies were different both between the different types of cancer cell and between the gel/co-gel types. Pure agarose provided the cells with 3D mechanical constraint without any adhesive ligands. In pure agarose, both the MDA-MB-231 and the HCT-116 cells grew into tumors with well-defined, smooth boundaries (Fig. 6(c) and (d), top rows). However, the HCT-116 cells more readily proliferated in this environment to form larger masses.

The presence of dense collagen nanofibers in the gels induced more proliferation from the MDA-MB-231 cells creating larger and more irregular mass shapes, which were punctuated by many long extended filopodia into the surrounding matrix showing a tendency of invasion (Fig. 6(c), second row). Interestingly, the addition of dense collagen nanofibers to the agarose gel did not have a significant effect on the mass size or morphology of HCT-116 cells (Fig. 6(d), second row). Large-scale confocal image volumes (Fig. 7(a)) facilitated the measurement of tumor volume, which was quantified for each cell and gel type and is presented in Fig. 7(b).

When cultured in agarose-collagen bundle co-gels, MDA-MB-231 cells formed two types of morphology depending on their location with respect to a collagen bundle (Fig. 6(c): third and fourth rows, Fig. 7(a)). In the case that they grew well away from a collagen bundle, their morphology was the same as in the agarose-collagen fiber gels. The second type of tumor morphology arose from cells that grew adjacent to a collagen bundle. They invaded and grew along the bundle as a cohort and formed long strands (mean length ± s.d.: 450 ± 375 μm) such that a tumor mass outside of the bundles was not present (Fig. 7(c)). The same observations held for the HCT-116 cells, however, to a lesser extent (Fig. 7(a) and (c)). When located near the collagen bundles, the HCT-116 cells tended to maintain tumor masses outside of the bundles—growing against the agarose matrix—with significantly shorter cell cohort protrusions (mean ± s.d.: 132 ± 116 μm) into the collagen bundles. This might be explained by the retention of the epithelial phenotype by the HCT-116 cells and the strong cell–cell junction strength due to high E-cadherin expression (Fig. S6).

Through the observations of the growth behaviors and morphologies of the two cancer cell lines we learned that invasive behaviors of cancer cells do not only require the presence of collagen, but also particular dimensions and structures of the collagen component provided by the collagen bundles. Furthermore, the MDA-MB-231 breast cancer cell line is known to be more aggressive and metastatic than the HCT-116 colon cancer cell line. The phenotypes of the two cell lines are recapitulated in our co-gels where the HCT-116 cells generally retained a more epithelial phenotype and corresponding markers (Fig. S6). Combining our microfluidic-driven alignment and the co-gel production, we were also able to demonstrate an agarose-collagen co-gel with complex collagen bundle patterns and the capability of repeatedly observing the tumor growth at the same locations in the co-gel (Fig. S8).

4. Discussion

In this study, we show a simple, rapid, and robust method of fabricating micro-scale, type I collagen bundles, which are not achievable using a traditional collagen gelling protocol. We showed that this method is applicable to type I collagen isolated from different species (bovine skin and rat tail). By varying temperature and ion content in the collagen precursor, we found high temperature and low ionic strength played key roles in the instant collagen bundle formation. As widely shown in *in vivo* studies, the tumor microenvironment often contains abundant microscale collagen fiber bundles that could directly guide cancer cell invasion as single cells or in a collective way [15]. This biological process may not be fully recapitulated by traditional collagen fiber gels due to the lack of the proper collagen architecture. Attempting to fill this gap, we evaluated how cancer cells interacted with our novel collagen bundles compared to traditional collagen nanofibers.

Making use of microfabrication and microfluidic techniques, we first demonstrated a novel and flexible way to post-process the collagen bundles into large-scale, controllable, and complex patterns with local alignment. The aligned bundles elicited migration behavior from cancer cells that was more directed and faster than in the isotropic collagen fiber gels. Whereas it has been shown that local collagen remodeling of collagen gels can enhance cancer cell invasion [7,14], our isotropic fiber gel trapped the cancer cells and impeded persistent migration. Pre-aligning our collagen fibers increased the directedness of migration to the level of the collagen bundles, however the migration speed was not increased. Slower migration along aligned fibers as compared to aligned bundles may be due to the difference in rigidity of the fibers at the length scale of the cell. The nanofibers can easily be deformed and buckled by the applied traction of the cells [3] whereas the larger collagen bundles present a more rigid substrate. The spacing between collagen bundles was a parameter that we have not yet attempted to vary, although doing so would allow more studies, such as probing of permissive and restrictive bundle arrangements for cell invasion. An example of such spacing effects is provided by a recent study in which it was found that the width of microtracks molded in collagen gels was related to the energy cost of cell migration with cells expending more energy to migrate in narrower tracks [57].

We then demonstrated the production of an agarose hydrogel embedded with collagen bundles. This co-gel differed from an earlier innovation of an agarose-collagen fiber co-gel [51] in the structure of the collagen. The previous co-gels provided new prospects for creating physiologically relevant models with controllable stiffness and collagen density. Here we add the important aspect of architectural factors. By controlling gelling temperature and ion content, we produced an agarose-collagen bundle co-gel and an

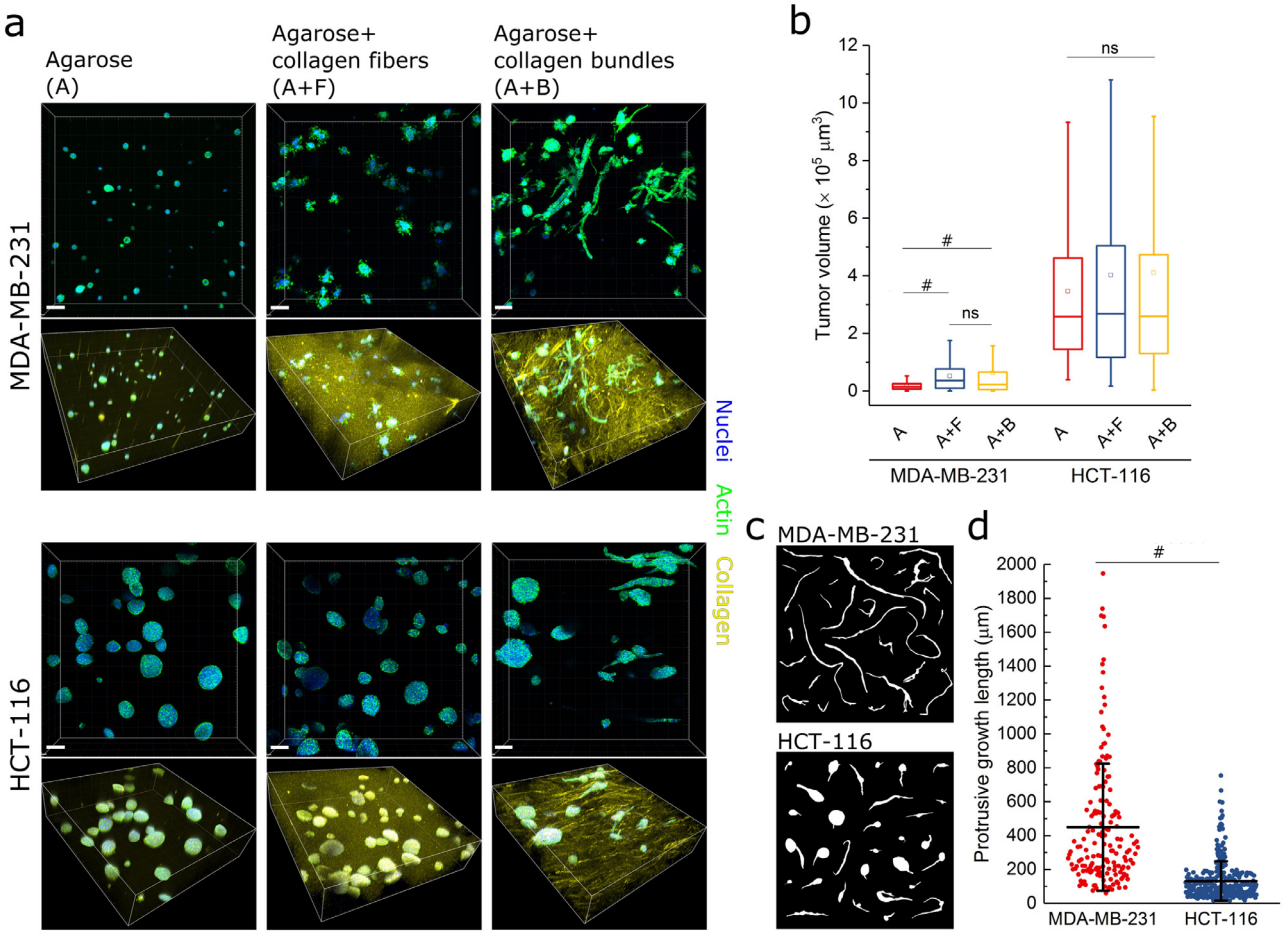

Fig. 7. Collagen bundles in agarose elicit cancer invasion. (a) Large scale 3D confocal imaging of MDA-MB-231 and HCT-116 tumors cultured for 10 days in pure agarose (A), agarose-collagen fiber co-gel (A + F), and agarose-collagen bundle co-gel (A + B). Scale bars: 100 μm. (b) Box plot showing tumor volume measurements of the two cell lines in the three gel conditions. One-way ANOVA with Tukey post hoc testing was used to compare the three gel conditions within each cell line. ($n \geq 326$ tumors for HCT-116; $n \geq 621$ tumors for MDA-MB-231) (c) Morphology of protrusive growth of both cell lines elicited by collagen bundles in the agarose-collagen bundle co-gels. (d) Protrusive growth length measurements of both cell lines (mean ± s.d). One-way ANOVA with Tukey post hoc testing, $n \geq 168$ protrusive growths, two samples each condition, # $p < 0.0001$, ns: no significance.

agarose-collagen fiber co-gel with comparable bulk stiffness at the same agarose concentration.

We compared pure agarose, agarose-collagen bundle co-gels, and agarose-collagen fiber co-gels as *in vitro* 3D tumor models. The growth of two cancer cell types with different metastatic potentials responded to the three gel types differently. Under the similar mechanical confinement—mainly provided by agarose—the presence of collagen and the collagen structures drastically influenced the behavior of invasive breast cancer cell MDA-MB-231. Although the presence of collagen nanofibers significantly enhanced the cell proliferation and elicited an invasive tendency of the mechanically constrained cells, cell invasion was hindered by the agarose mesh. On the other hand, in the collagen bundle-containing agarose, cancer cells formed multicellular cohorts along the collagen, which resembled collective invasion as seen *in vivo* [15]. In comparison with MDA-MB-231 cells, human colon cancer cells HCT-116, with strong cell-cell adhesion, did not appear to have as pronounced of an invasive tendency when surrounded by collagen nanofibers. However, in the agarose-collagen bundle co-gel, distinct cell-cohort protrusions originating from HCT-116 tumor spheroids were observed when the growing tumors made contact with the collagen bundles.

Traditional methods of making nanoscale collagen fibers with variable fiber thickness have been well-established and are reproducible. With the characterizations of cancer cell motility and invading capability, our novel yet simple method of rapidly producing microscale collagen bundles adds another level of collagen structure that may be incorporated into *in vitro* tumor models. The collagen bundle-based *in vitro* models may be used to better understand the underlying mechanism of cell invasion along collagen bundles and in fibrotic stroma. Not only may the collagen bundles be applied to study cancer cell phenotypes and metastasis, but also provide new avenues for tissue engineering using a natural tissue component—collagen—as scaffolds. For example, aligned microscale bundled collagen may provide biocompatibility, adhesion, and proper topography for skeletal muscle growth [58,59] and nerve regeneration [60,61].

5. Conclusion

In summary, we have developed a novel and simple fabrication method to rapidly produce microscale collagen bundles. These collagen bundles could be aligned by a microfluidic device or embedded within an agarose hydrogel. The aligned collagen bundles, which mimicked tumor-associated collagen architectures, were shown to elicit cancer cells' contact guidance and enhance their directional migration. In agarose-collagen co-gels, we showed that two different cancer cell types responded to collagen structures differently, and that microscale collagen structures were required for both cell types to invade. Overall, we believe the use

of the microscale collagen bundles will help to elucidate the significant role of stromal collagen structure in cancer cell behavior. This study has expanded the controllability of reconstituted collagen structure, and therefore provided a possibility of creating more physiologically relevant *in vitro* 3D models.

Declaration of Competing Interest

The authors declare no competing interests.

Acknowledgments

We thank Jamie Gearhart in the Mills Lab for the help with the mechanical testing on the hydrogels. We thank Prof. Lee Ligon for the helpful discussion. We acknowledge Dr. Sergey Pryshchep's assistance on confocal microscopy, the National Science Foundation (Grant # NSF-MRI-1725984), and the software access (Imaris) in the Biotech Microscopy Core at Rensselaer Polytechnic Institute (RPI). We also thank M. David Frey for his technical assistance with scanning electron microscopy performed in the Micro and Nano Fabrication Clean Room (MNCR) at RPI. This work is supported by start-up funding for Dr. Mills's lab from RPI.

Supplementary materials

Supplementary material associated with this article can be found, in the online version, at doi:10.1016/j.actbio.2020.03.019.

References

[1] C.M. Nelson, M.J. Bissell, Of extracellular matrix, scaffolds, and signaling: tissue architecture regulates development, homeostasis, and cancer, Annu. Rev. Cell Dev. Biol. 22 (2006) 287–309.
[2] N.J. Hogrebe, J.W. Reinhardt, K.J. Gooch, Biomaterial microarchitecture: a potent regulator of individual cell behavior and multicellular organization, J. Biomed. Mater. Res. A. 105 (2017) 640–661.
[3] Y.L. Han, P. Ronceray, G. Xu, A. Malandrino, R.D. Kamm, M. Lenz, C.P. Broedersz, M. Guo, Cell contraction induces long-ranged stress stiffening in the extracellular matrix, Proc. Natl. Acad. Sci. 115 (2018) 4075–4080.
[4] Y.-Q. Chen, J.-C. Kuo, M.-T. Wei, Y.-C. Chen, M.-H. Yang, A. Chiou, Early stage mechanical remodeling of collagen surrounding head and neck squamous cell carcinoma spheroids correlates strongly with their invasion capability, Acta Biomater. 84 (2019) 280–292.
[5] Q. Xiao, G. Ge, Lysyl oxidase, extracellular matrix remodeling and cancer metastasis, Cancer Microenviron. Off. J. Int. Cancer Microenviron. Soc. 5 (2012) 261–273.
[6] K.R. Levental, H. Yu, L. Kass, J.N. Lakins, M. Egeblad, J.T. Erler, S.F.T. Fong, K. Csiszar, A. Giaccia, W. Weninger, M. Yamauchi, D.L. Gasser, V.M. Weaver, Matrix crosslinking forces tumor progression by enhancing integrin signaling, Cell 139 (2009) 891–906.
[7] K. Wolf, Y.I. Wu, Y. Liu, J. Geiger, E. Tam, C. Overall, M.S. Stack, P. Friedl, Multi--step pericellular proteolysis controls the transition from individual to collective cancer cell invasion, Nat. Cell Biol. 9 (2007) 893–904.
[8] K.B. Pointer, P.A. Clark, A.B. Schroeder, M.S. Salamat, K.W. Eliceiri, J.S. Kuo, Association of collagen architecture with glioblastoma patient survival, J. Neurosurg. 126 (2017) 1812–1821.
[9] M.-F. Penet, S. Kakkad, A.P. Pathak, B. Krishnamachary, Y. Mironchik, V. Raman, M. Solaiyappan, Z.M. Bhujwalla, Structure and function of a prostate cancer dissemination-permissive extracellular matrix, Clin. Cancer Res. Off. J. Am. Assoc. Cancer Res. 23 (2017) 2245–2254.
[10] I. Acerbi, L. Cassereau, I. Dean, Q. Shi, A. Au, C. Park, Y.Y. Chen, J. Liphardt, E.S. Hwang, V.M. Weaver, Human breast cancer invasion and aggression correlates with ECM stiffening and immune cell infiltration, Integr. Biol. Quant. Biosci. Nano Macro 7 (2015) 1120–1134.
[11] W. Han, S. Chen, W. Yuan, Q. Fan, J. Tian, X. Wang, L. Chen, X. Zhang, W. Wei, R. Liu, J. Qu, Y. Jiao, R.H. Austin, L. Liu, Oriented collagen fibers direct tumor cell intravasation, Proc. Natl. Acad. Sci. 113 (2016) 11208–11213.
[12] M.W. Conklin, P.J. Keely, Why the stroma matters in breast cancer, Cell Adhes. Migr. 6 (2012) 249–260.
[13] P.P. Provenzano, K.W. Eliceiri, J.M. Campbell, D.R. Inman, J.G. White, P.J. Keely, Collagen reorganization at the tumor-stromal interface facilitates local invasion, BMC Med. 4 (2006) 38.
[14] P.P. Provenzano, D.R. Inman, K.W. Eliceiri, S.M. Trier, P.J. Keely, Contact guidance mediated three-dimensional cell migration is regulated by rho/rock-dependent matrix reorganization, Biophys. J. 95 (2008) 5374–5384.
[15] M. Chanrion, I. Kuperstein, C. Barrière, F.E. Marjou, D. Cohen, D. Vignjevic, L. Stimmer, P. Paul-Gilloteaux, I. Bièche, S.D.R. Tavares, G.-F. Boccia, W. Cacheux, D. Meseure, S. Fre, L. Martignetti, P. Legoix-Né, E. Girard, L. Fetler, E. Barillot, D. Louvard, A. Zinovyev, S. Robine, Concomitant Notch activation and p53 deletion trigger epithelial-to-mesenchymal transition and metastasis in mouse gut, Nat. Commun. 5 (2014) 5005.
[16] K.S. Kopanska, Y. Alcheikh, R. Staneva, D. Vignjevic, T. Betz, Tensile forces originating from cancer spheroids facilitate tumor invasion, PLoS ONE 11 (2016) e0156442.
[17] Y.A. Miroshnikova, G.I. Rozenberg, L. Cassereau, M. Pickup, J.K. Mouw, G. Ou, K.L. Templeman, E.-I. Hannachi, K.J. Gooch, A.L. Sarang-Sieminski, A.J. García, V.M. Weaver, $\alpha 5\beta 1$-Integrin promotes tension-dependent mammary epithelial cell invasion by engaging the fibronectin synergy site, Mol. Biol. Cell 28 (2017) 2958–2977.
[18] E. Brown, T. McKee, E. diTomaso, A. Pluen, B. Seed, Y. Boucher, R.K. Jain, Dynamic imaging of collagen and its modulation in tumors *in vivo* using second-harmonic generation, Nat. Med. 9 (2003) 796–800.
[19] F. Kai, A.P. Drain, V.M. Weaver, The extracellular matrix modulates the metastatic journey, Dev. Cell 49 (2019) 332–346.
[20] D. Chen, G. Chen, W. Jiang, M. Fu, W. Liu, J. Sui, S. Xu, Z. Liu, X. Zheng, L. Chi, D. Lin, K. Li, W. Chen, N. Zuo, J. Lu, J. Chen, G. Li, S. Zhuo, J. Yan, Association of the collagen signature in the tumor microenvironment with lymph node metastasis in early gastric cancer, JAMA Surg. 154 (2019) e185249.
[21] S.M. Kakkad, M. Solaiyappan, P. Argani, S. Sukumar, L.K. Jacobs, D. Leibfritz, Z.M. Bhujwalla, K. Glunde, Collagen i fiber density increases in lymph node positive breast cancers: pilot study,, J. Biomed. Opt. 17 (2012) 116017.
[22] M.W. Conklin, R.E. Gangnon, B.L. Sprague, L. Van Gemert, J.M. Hampton, K.W. Eliceiri, J.S. Bredfeldt, Y. Liu, N. Surachaicharn, P.A. Newcomb, A. Friedl, P.J. Keely, A. Trentham-Dietz, Collagen alignment as a predictor of recurrence after ductal carcinoma in situ, Cancer Epidemiol. Biomark. Prev. Publ. Am. Assoc. Cancer Res. Cosponsored Am. Soc. Prev. Oncol. 27 (2018) 138–145.
[23] M.J. Paszek, N. Zahir, K.R. Johnson, J.N. Lakins, G.I. Rozenberg, A. Gefen, C.A. Reinhart-King, S.S. Margulies, M. Dembo, D. Boettiger, D.A. Hammer, V.M. Weaver, Tensional homeostasis and the malignant phenotype, Cancer Cell 8 (2005) 241–254.
[24] G. Rijal, W. Li, 3D scaffolds in breast cancer research, Biomaterials 81 (2016) 135–156.
[25] P. Fratzl, Collagen: structure and mechanics, an introduction, in: P. Fratzl (Ed.), Collagen: Structure and Mechanics, Springer US, Boston, MA, 2008, pp. 1–13. h.
[26] A.O. Brightman, B.P. Rajwa, J.E. Sturgis, M.E. McCallister, J.P. Robinson, S.L. Voytik-Harbin, Time-lapse confocal reflection microscopy of collagen fibrillogenesis and extracellular matrix assembly *in vitro*, Biopolymers 54 (2000) 222–234.
[27] L. He, W. Chen, P.-H. Wu, A. Jimenez, B.S. Wong, A. San, K. Konstantopoulos, D. Wirtz, Local 3D matrix confinement determines division axis through cell shape, Oncotarget 7 (2016) 6994–7011.
[28] S.I. Fraley, Y. Feng, R. Krishnamurthy, D.-H. Kim, A. Celedon, G.D. Longmore, D. Wirtz, A distinctive role for focal adhesion proteins in three-dimensional cell motility, Nat. Cell Biol. 12 (2010) 598–604.
[29] S.I. Fraley, P. Wu, L. He, Y. Feng, R. Krisnamurthy, G.D. Longmore, D. Wirtz, Three-dimensional matrix fiber alignment modulates cell migration and MT1-MMP utility by spatially and temporally directing protrusions, Sci. Rep. 5 (2015) 14580.
[30] J. Sapudom, S. Rubner, S. Martin, T. Kurth, S. Riedel, C.T. Mierke, T. Pompe, The phenotype of cancer cell invasion controlled by fibril diameter and pore size of 3D collagen networks, Biomaterials 52 (2015) 367–375.
[31] E.E. Antoine, P.P. Vlachos, M.N. Rylander, Tunable collagen i hydrogels for engineered physiological tissue micro-environments, PLoS ONE 10 (2015) e0122500.
[32] A.D. Doyle, N. Carvajal, A. Jin, K. Matsumoto, K.M. Yamada, Local 3D matrix microenvironment regulates cell migration through spatiotemporal dynamics of contractility-dependent adhesions, Nat. Commun. 6 (2015) 8720.
[33] S.P. Carey, C.M. Kraning-Rush, R.M. Williams, C.A. Reinhart-King, Biophysical control of invasive tumor cell behavior by extracellular matrix microarchitecture, Biomaterials 33 (2012) 4157–4165.
[34] C. Guo, L.J. Kaufman, Flow and magnetic field induced collagen alignment, Biomaterials 28 (2007) 1105–1114.
[35] K.M. Riching, B.L. Cox, M.R. Salick, C. Pehlke, A.S. Riching, S.M. Ponik, B.R. Bass, W.C. Crone, Y. Jiang, A.M. Weaver, K.W. Eliceiri, P.J. Keely, 3D Collagen alignment limits protrusions to enhance breast cancer cell persistence, Biophys. J. 107 (2014) 2546–2558.
[36] P. Lee, R. Lin, J. Moon, L.P. Lee, Microfluidic alignment of collagen fibers for *in vitro* cell culture, Biomed. Microdev. 8 (2006) 35–41.
[37] J.S. McLane, C.J. Rivet, R.J. Gilbert, L.A. Ligon, A biomaterial model of tumor stromal microenvironment promotes mesenchymal morphology but not epithelial to mesenchymal transition in epithelial cells, Acta Biomater. 10 (2014) 4811–4821.
[38] A. Williams, J.F. Nowak, R. Dass, J. Samuel, K.L. Mills, Toward morphologically relevant extracellular matrix in vitro models: 3D fiber reinforced hydrogels, Front. Physiol. (2018) 9.
[39] G.A.D. Lullo, S.M. Sweeney, J. Körkkö, L. Ala-Kokko, J.D.S. Antonio, Mapping the ligand-binding sites and disease-associated mutations on the most abundant protein in the human, type I collagen, J. Biol. Chem. 277 (2002) 4223–4231.
[40] A. Ray, O. Lee, Z. Win, R.M. Edwards, P.W. Alford, D.-H. Kim, P.P. Provenzano, Anisotropic forces from spatially constrained focal adhesions mediate contact guidance directed cell migration, Nat. Commun. 8 (2017) 14923.

[41] E.D. Tabdanov, V. Puram, A. Zhovmer, P.P. Provenzano, Microtubule-actomyosin mechanical cooperation during contact guidance sensing, Cell Rep. 25 (2018) 328–338 e5.
[42] S.H. Kim, S.-.K. Im, S.-J. Oh, S. Jeong, E.-.S. Yoon, C.J. Lee, N. Choi, E.-.M. Hur, Anisotropically organized three-dimensional culture platform for reconstruction of a hippocampal neural network, Nat. Commun. 8 (2017) 14346.
[43] N. Rajan, J. Habermehl, M.-.F. Coté, C.J. Doillon, D. Mantovani, Preparation of ready-to-use, storable and reconstituted type I collagen from rat tail tendon for tissue engineering applications, Nat. Protoc 1 (2006) 2753–2758.
[44] L. Rittié, Type i collagen purification from rat tail tendons, in: L. Rittié (Ed.), Fibrosis Methods and Protocols, Springer New York, New York, NY, 2017, pp. 287–308.
[45] D. Qin, Y. Xia, G.M. Whitesides, Soft lithography for micro- and nanoscale patterning, Nat. Protoc. 5 (2010) 491–502.
[46] A.G. Pogorelov, I.I. Selezneva, Evaluation of collagen gel microstructure by scanning electron microscopy, Bull. Exp. Biol. Med 150 (2010) 153–156.
[47] C.A. Schneider, W.S. Rasband, K.W. Eliceiri, NIH image to imageJ: 25 years of image analysis, Nat. Methods 9 (2012) 671–675.
[48] C. Steger, An unbiased detector of curvilinear structures, IEEE Trans. Pattern Anal. Mach. Intell. 20 (1998) 113–125.
[49] R. Rezakhaniha, A. Agianniotis, J.T.C. Schrauwen, A. Griffa, D. Sage, C.V.C. Bouten, F.N. van de Vosse, M. Unser, N. Stergiopulos, Experimental investigation of collagen waviness and orientation in the arterial adventitia using confocal laser scanning microscopy, Biomech. Model. Mechanobiol. 11 (2012) 461–473.
[50] R. Li, J.D. Hebert, T.A. Lee, H. Xing, A. Boussommier-Calleja, R.O. Hynes, D.A. Lauffenburger, R.D. Kamm, Macrophage-Secreted TNFα and TGFβ1 influence migration speed and persistence of cancer cells in 3D tissue culture via independent pathways, Cancer Res 77 (2017) 279–290.
[51] T.A. Ulrich, A. Jain, K. Tanner, J.L. MacKay, S. Kumar, Probing cellular mechanobiology in three-dimensional culture with collagen–agarose matrices, Biomaterials 31 (2010) 1875–1884.
[52] A.J. Berger, K.M. Linsmeier, P.K. Kreeger, K.S. Masters, Decoupling the effects of stiffness and fiber density on cellular behaviors via an interpenetrating network of gelatin-methacrylate and collagen, Biomaterials 141 (2017) 125–135.
[53] D.T. Butcher, T. Alliston, V.M. Weaver, A tense situation: forcing tumour progression, Nat. Rev. Cancer 9 (2009) 108–122.
[54] G. Helmlinger, P.A. Netti, H.C. Lichtenbeld, R.J. Melder, R.K. Jain, Solid stress inhibits the growth of multicellular tumor spheroids, Nat. Biotechnol. 15 (1997) 778–783.
[55] C.-.C. Chou, K.-.H. Lee, I.-.L. Lai, D. Wang, X. Mo, S.K. Kulp, C.L. Shapiro, C.-.S. Chen, AMPK reverses the mesenchymal phenotype of cancer cells by targeting the AKT–MDM2–FOXO3A signaling axis, Cancer Res. 74 (2014) 4783–4795.
[56] K. Hur, Y. Toiyama, M. Takahashi, F. Balaguer, T. Nagasaka, J. Koike, H. Hemmi, M. Koi, C.R. Boland, A. Goel, MicroRNA-200c modulates epithelial-to-mesenchymal transition (EMT) in human colorectal cancer metastasis, Gut 62 (2013) 1315–1326.
[57] M.R. Zanotelli, A. Rahman-Zaman, J.A. VanderBurgh, P.V. Taufalele, A. Jain, D. Erickson, F. Bordeleau, C.A. Reinhart-King, Energetic costs regulated by cell mechanics and confinement are predictive of migration path during decision–making, Nat. Commun. 10 (2019) 1–12.
[58] K.J. Aviss, J.E. Gough, S. Downes, Aligned electrospun polymer fibres for skeletal muscle regeneration, Eur. Cell. Mater. 19 (2010) 193–204.
[59] M. Yeo, G.H. Kim, Anisotropically aligned cell-laden nanofibrous bundle fabricated via cell electrospinning to regenerate skeletal muscle tissue, Small 14 (2018) 1803491.
[60] A. Subramanian, U.M. Krishnan, S. Sethuraman, Development of biomaterial scaffold for nerve tissue engineering: biomaterial mediated neural regeneration, J. Biomed. Sci. 16 (2009) 108.
[61] N.J. Schaub, C.D. Johnson, B. Cooper, R.J. Gilbert, Electrospun fibers for spinal cord injury research and regeneration, J. Neurotrauma 33 (2016) 1405–1415.